Giant Terahertz-Wave Absorption by Monolayer Graphene in a Total Internal Reflection Geometry

Yoichi Harada,[†,‡] Muhammad Shoufie Ukhtary,[¶] Minjie Wang,[†] Sanjay K. Srinivasan,[†,§] Eddwi H. Hasdeo,[¶] Ahmad R. T. Nugraha,[¶] G. Timothy Noe II,[†] Yuji Sakai,[∥] Robert Vajtai,[⊥] Pulickel M. Ajayan,[⊥] Riichiro Saito,[¶] and Junichiro Kono[*,†,#,⊥]

Department of Electrical and Computer Engineering, Rice University, Houston, Texas 77005, United States, Department of Engineering, Hokkaido University, Sapporo 060-8628, Japan, Department of Physics, Tohoku University, Sendai 980-8578, Japan, Department of Physics and Nanotechnology, SRM University, Kancheepuram District, Chennai, Tamil Nadu, 603203, India, Institute of Laser Engineering, Osaka University, Suita, 565-0871, Japan, Department of Materials Science and NanoEngineering, Rice University, Houston, Texas 77005, United States, and Department of Physics and Astronomy, Rice University, Houston, Texas 77005, United States

E-mail: kono@rice.edu

Abstract

We experimentally demonstrated significant enhancement of terahertz-wave absorption in monolayer graphene by simply sandwiching monolayer graphene between two dielectric media in a total internal reflection geometry. In going through this structure, the evanescent wave of the incident terahertz beam interacts with the sandwiched graphene layer multiple (up to four) times at varying incidence angles. We observed extremely large attenuation (up to $\sim 70\%$ per reflection), especially for *s*-polarized radiation. The experimental results are quantitatively consistent with our calculations, where we modeled the experiment as an electromagnetic wave reflection process in monolayer graphene. We also derived analytical expressions for the absorptance, showing that the absorptance is proportional to the amount of Joule heating on the graphene surface induced by the terahertz radiation.

Keywords: graphene, terahertz spectroscopy, absorption, total internal reflection

*To whom correspondence should be addressed

†Department of Electrical and Computer Engineering, Rice University, Houston, Texas 77005, United States

‡Department of Engineering, Hokkaido University, Sapporo 060-8628, Japan

¶Department of Physics, Tohoku University, Sendai 980-8578, Japan

§Department of Physics and Nanotechnology, SRM University, Kancheepuram District, Chennai, Tamil Nadu, 603203, India

‖Institute of Laser Engineering, Osaka University, Suita, 565-0871, Japan

⊥Department of Materials Science and NanoEngineering, Rice University, Houston, Texas 77005, United States

#Department of Physics and Astronomy, Rice University, Houston, Texas 77005, United States

The gapless and massless band structure and widely tunable Fermi energy of graphene are expected to lead to unconventional high-frequency phenomena and devices that can impact the science and technology of terahertz (THz) radiation.[1–3] Because of the inherently small interaction lengths in atomically thin systems, interband absorption in graphene is minuscule, whereas *intraband* absorption for a normal incidence THz beam can be as large as $\sim 20\%$ per layer, depending on the carrier density.[4–9] Different approaches have been suggested for enhancing absorption in monolayer graphene,[10–12] both in the optical and THz ranges, but most of them require complicated structures, such as grating couplers and/or graphene nanoribbons/nanodiscs.

Ukhtary *et al.* have recently proposed a simple and robust method for enhancing THz absorption in graphene using a total internal reflection (TIR) geometry.[13] In their proposed scheme, a graphene monolayer is placed at the interface of two dielectric media, and the THz wave is incident onto the interface with an incidence angle, θ, larger than the critical angle, θ_c, for TIR. By varying the Fermi energy, E_F, the absorption probability can be arbitrarily tuned between 100% and 0%. Here, we report an experimental demonstration of this proposed scheme for THz absorption enhancement. Our unique 'graphene-on-TOPAS' waveguide structure (Figure 1) allows the incident THz beam to be absorbed by monolayer graphene multiple times at various θ ($> \theta_c$). We observed extremely large THz absorption, leading to total attenuation, especially for *s*-polarized radiation. The observed absorption amount, as well as its dependence on θ, can be quantitatively reproduced by our calculations, incorporating realistic values of E_F and the carrier scattering time, τ.

As the two adjoining media, we chose TOPAS® (Thermoplastic Olefin Polymer of Amorphous Structure), which has a negligible absorption coefficient and constant refractive index ($n_1 = 1.523 \pm 0.002$) throughout the THz range,[14] and air ($n_2 = 1$). Hence, $\theta_c = \sin^{-1}(n_2/n_1) = 41.06°$. Figure 1(a) schematically shows the design of our graphene-on-TOPAS waveguide and the corresponding beam path for the case of $\theta = 45°$. We combined two parallelogram-shaped TOPAS prisms, which created six TOPAS/air interfaces; two of

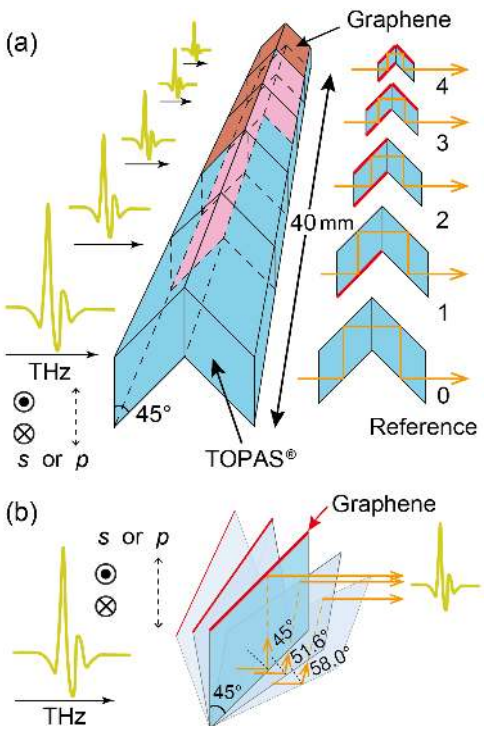

Figure 1: Sketch of the graphene-on-TOPAS waveguide geometry. (a) Two pieces of TOPAS® parallelograms are combined for four 45-degree reflections. One, two, three, or four pieces of graphene are put on the surfaces of TOPAS®. Different numbers of graphene reflections can be selected by sliding the structure in a direction perpendicular to the incident THz beam. (b) One-parallelogram geometry for angular dependence measurements. The incidence angle to graphene is controlled by the rotatable stage under the waveguide.

the interfaces were uncovered and normal to the incident/transmitted THz beam, while a specific number (1, 2, 3, or 4) of the other four were covered by graphene. A linear translation stage allowed us to slide the waveguide structure in a direction perpendicular to the beam propagation direction, enabling measurements of the transmitted THz intensity, $I^{(n)}$, after $n = 0$, 1, 2, 3, and 4 reflections by graphene. The transmission signal with no graphene, $I^{(0)}$, was used as a reference to calculate the relative transmittance, $T_{\mathrm{TOPAS+G}}/T_{\mathrm{TOPAS}}$, where $T_{\mathrm{TOPAS+G}}$ (T_{TOPAS}) is the transmittance of the waveguide structure with (without) graphene. In all measurements, the THz wave was linearly polarized, and therefore, by turning the waveguide structure by 90° in a plane perpendicular to the beam, we were able to perform transmission measurements for either a p- or s-polarized THz beam. Furthermore, in

order to investigate the incidence-angle dependence of graphene absorption, we used a one-parallelogram TOPAS geometry, shown in Figure 1(b), where θ was manually changeable by rotating the whole waveguide structure in a plane parallel to the beam. The electric field strength of the THz wave was less than 10 V/cm. This low electric field strength ensures that we can neglect any electron thermalization effects that can lead to nonlinear THz response.[9]

Large-area graphene samples used in this study were grown by chemical vapor deposition. In order to characterize the samples in the THz and infrared ranges, we used THz time-domain spectroscopy (see Methods) and Fourier-transform infrared spectroscopy (JASCO FT/IR-660 Plus). The measured optical conductivity was fit with the Drude conductivity, $\sigma(\omega) = \sigma_0/(1 - i\omega\tau)$, where σ_0 is the DC conductivity and τ is relaxation time. Figure 2 shows the real part of the optical conductivity calculated from experimental transmittance data for a graphene sample on a TOPAS substrate, together with a fitting curve using the real part of the Drude conductivity, $\sigma' = \sigma_0/(1 + \omega^2\tau^2)$. The refractive index of TOPAS was used for converting the transmittance to the optical conductivity. Through the best fit to the data, we obtained $\sigma_0 = 1.04 \times 10^{-3} \pm 0.01\,\mathrm{S/m}$ and $\tau = 28.8 \pm 0.2\,\mathrm{fs}$. In addition, through $\sigma_0 = en_\mathrm{s}\mu$, $\mu = (ev_\mathrm{F}\tau)/(\hbar k_\mathrm{F})$, $k_\mathrm{F} = \sqrt{\pi n_\mathrm{s}}$, and $E_\mathrm{F} = v_\mathrm{F}\hbar k_\mathrm{F}$, we obtained the sheet carrier density $n_\mathrm{s} = 6.08 \times 10^{16}\,\mathrm{m}^{-2}$, carrier mobility $\mu = 1.07 \times 10^3\,\mathrm{cm}^2/\mathrm{Vs}\,(0.107\,\mathrm{m}^2/\mathrm{Vs})$, and $E_\mathrm{F} = 0.308\,\mathrm{eV}$. Here, e is the electronic charge, k_F is the Fermi wavenumber, and v_F is the Fermi velocity of graphene, $1.07 \times 10^6\,\mathrm{m/s}$.[15]

Figures 3(a) and (b) show spectra of relative transmittance, $T_\mathrm{TOPAS+G}/T_\mathrm{TOPAS}$, for different numbers of graphene layers on the TOPAS waveguide for p- and s-polarized THz waves, respectively, up to four layers. After spectral averaging over the range of 0.5-1.5 THz, we found that 28.2% of the incident wave was absorbed by graphene at each reflection for a p-polarized THz wave, $(1 - 0.282)^4 = 26.2\%$ remaining after four reflections. On the other hand, in the case of s-polarization, 71.0% of the incident wave was absorbed by graphene at each reflection, only $(1 - 0.710)^4 = 0.7\%$ remaining after four reflections. The constancy of absorption per reflection can be clearly seen in Figure 3(c), where $(T_\mathrm{TOPAS+G}/T_\mathrm{TOPAS})^{1/n}$

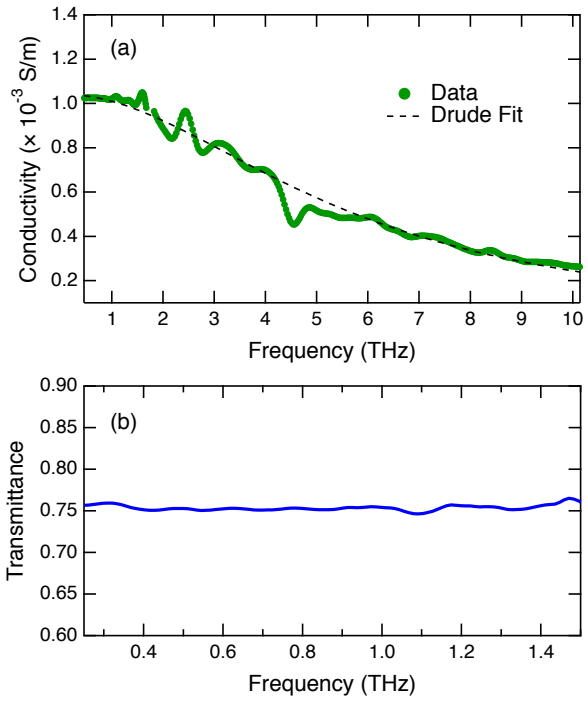

Figure 2: (a) The real part of the optical conductivity measured for a large-area monolayer graphene sample grown by chemical vapor deposition and transferred onto a TOPAS substrate. The black dashed curve shows a fit to the Drude model. (b) Transmittance of graphene on TOPAS for normal incidence in the THz range.

is plotted for $n = 1, 2, 3, 4$ for both p- and s-polarized beams. Finally, Figure 3(d) shows theoretically calculated spectra that reproduce the experimental spectra using the values of E_{F} and τ for this graphene sample. Details of our theoretical model are described later.

Finally, we carried out detailed incident-angle-dependent measurements by rotating the waveguide [see Figure 1(b)]. Figure 4(a) shows the dependence of the spectrally averaged transmittance value measured as a function of θ for p- and s-polarized THz waves. There is strong angular dependence for both polarizations, and the angular dependence is strongly polarization dependent. For p-polarization, the transmittance value right above the critical angle is higher than 0.9, indicating the absorption by graphene is small. However, with increasing θ, the transmittance (absorptance) decreases (increases), reaching 0.61 (0.39) at $\theta = 55°$. Above 55°, the transmittance (absorptance) then increases (decreases) and becomes

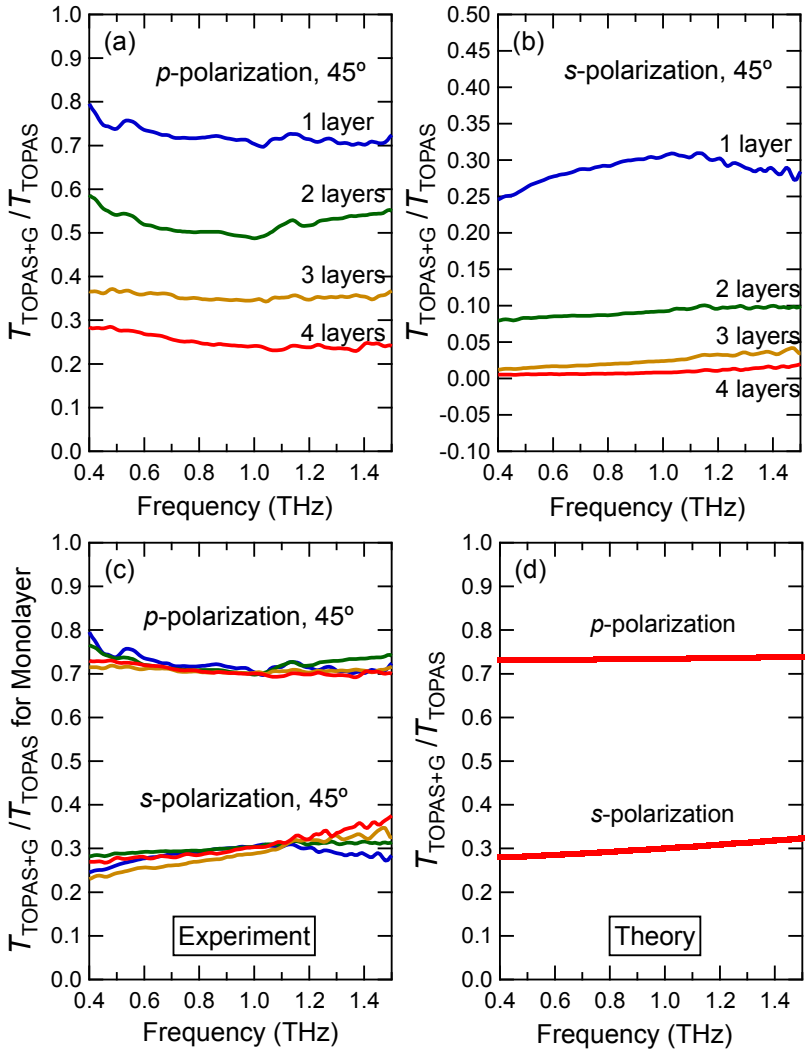

Figure 3: Transmission of a THz wave through the graphene-on-TOPAS structure at an incident angle of 45° at each of the four total internal reflections. (a) Transmittance spectra for the structure for a *p*-polarized THz wave. (b) Transmittance spectra for the structure for an *s*-polarized THz wave. (c) Transmittance spectra for a single reflection by monolayer graphene for both *s*- and *p*-polarized THz waves. (d) Theoretically calculated transmittance spectra to simulate the data in (c).

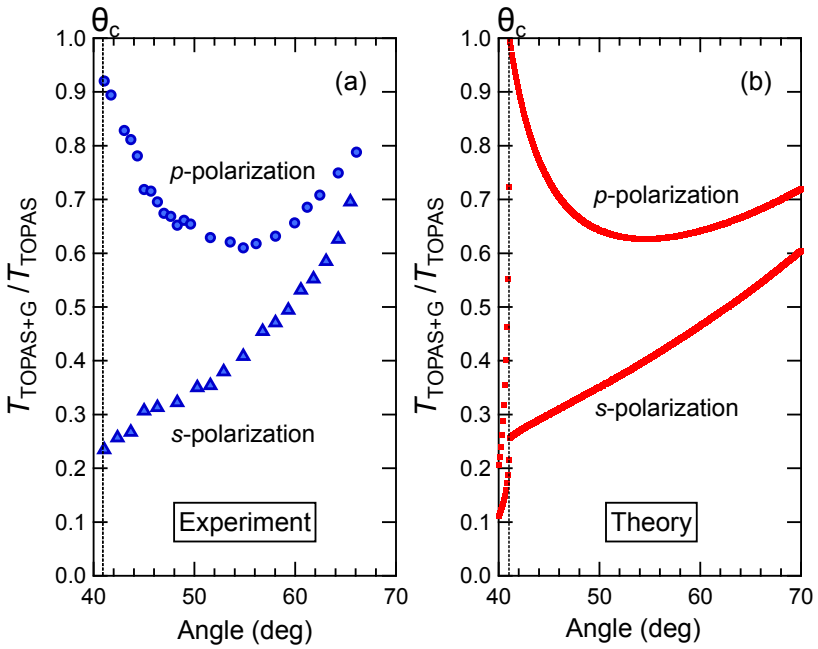

Figure 4: (a) Experimental and (b) theoretical angular dependence of THz transmittance through the graphene-on TOPAS waveguide structure for p- and s-polarized THz waves. There is strong angular dependence for both polarizations, and the angular dependence is qualitatively different between the two polarizations, which are reproduced in the theoretical calculations.

$\sim$0.8 ($\sim$0.2) at 66°. In the case of s-polarized THz waves, the absorptance is 76.5% right above the critical angle and then monotonically decreases with increasing θ, reaching 30.4% at 66°. Below, we describe our theoretical model in detail, which correctly reproduced the observed angular dependence, as shown in Figure 4(b).

The experiments above can be modeled as a reflection process on monolayer graphene. The experimentally obtained relative transmittance of the TOPAS structure, $T_{\rm TOPAS+G}/T_{\rm TOPAS}$ can be reproduced theoretically by calculating the reflection probability [R_p (R_s) for p (s)-polarized wave] of monolayer graphene. Suppose we have monolayer graphene placed between TOPAS and air, with refractive indexes $n_1 = 1.523$ and $n_2 = 1$, respectively and a THz wave coming to graphene at angle θ as shown in Figure 5. A portion of the wave is reflected back to TOPAS at angle θ, another portion refracted into the air at angle ϕ, and the rest is absorbed by monolayer graphene. The process is shown in Figure 5, where E_i (H_i) is the

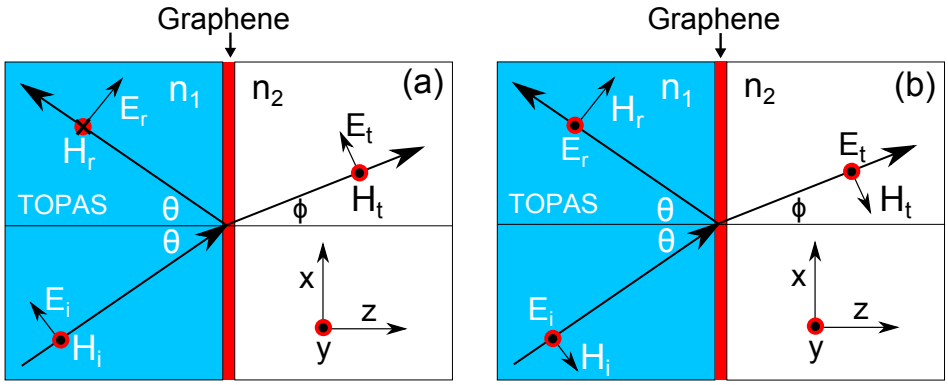

Figure 5: Our theoretical model: graphene is surrounded by two media, $n_1 = 1.523$ and $n_2 = 1$. (a) p-polarized and (b) s-polarized THz wave are incident on the graphene surface with angle θ.

incident electric (magnetic) field, E_t (H_t) is the transmitted electric (magnetic) field, and E_r (H_r) is the reflected electric (magnetic) field.

Let us focus on $\theta \geq \theta_c$, where the wave is not refracted to air; instead it can only be reflected back to TOPAS or absorbed by monolayer graphene. Note that an evanescent wave will exist at the TOPAS-graphene-air boundary. The reflection probability (R_p and R_s) of the incident wave can be calculated by employing appropriate boundary conditions. Figure 5 shows the geometrical setup of our model for p- and s-polarized waves incident on graphene. The boundary conditions are such that the electric fields on the surface of graphene are continuous, while the magnetic fields are not, due to the presence of surface current density. The boundary conditions can be written as

$$\begin{aligned} E_i \cos\theta + E_r \cos\theta &= E_t \cos\phi \\ H_t - (H_i - H_r) &= -\sigma E_t \cos\phi, \end{aligned} \tag{1}$$

for p-polarization and

$$E_i + E_r = E_t$$
$$H_t \cos\phi - (H_i \cos\theta - H_r \cos\theta) = \sigma E_t, \tag{2}$$

for s-polarization, where the current density on the graphene surface is denoted by $\sigma E_t \cos\phi$ (σE_t) for p (s)-polarization and σ is graphene's complex optical conductivity. By solving Eqs. (1) and (2) for $r_k \equiv (E_r/E_i)_k$, where k is a polarization index ($k = p, s$), we have

$$r_p = \frac{Z_2 \cos\phi - Z_1 \cos\theta - \sigma Z_1 Z_2 \cos\theta \cos\phi}{Z_2 \cos\phi + Z_1 \cos\theta + \sigma Z_1 Z_2 \cos\theta \cos\phi} \tag{3}$$
$$r_s = \frac{Z_2 \cos\theta - Z_1 \cos\phi - \sigma Z_1 Z_2}{Z_2 \cos\theta + Z_1 \cos\phi + \sigma Z_1 Z_2} \tag{4}$$
$$R_p = |r_p|^2 \tag{5}$$
$$R_s = |r_s|^2, \tag{6}$$

where θ and ϕ are related to each other through Snell's law, $Z_2 \sin\theta = Z_1 \sin\phi$, and Z_l ($l = 1, 2$) is the wave impedance for Medium l, defined as

$$Z_l = \frac{E}{H} = \frac{377}{n_l}\ \Omega. \tag{7}$$

It should be noted that the critical angle θ_c is defined through $\sin\theta_c = Z_1/Z_2$ and that $\cos\phi = \sqrt{1 - (\frac{\sin\theta}{\sin\theta_c})^2}$ is purely imaginary if $\theta > \theta_c$. In this case, the THz wave is evanescent in vacuum ($E \propto e^{-\kappa z}$) with decay length $\frac{1}{\kappa} = \frac{\lambda_0}{2\pi\sqrt{(\frac{\sin\theta}{\sin\theta_c})^2 - 1}}$, where λ_0 is the THz wavelength in vacuum; for example, in the case of Figure 1(a) with $\theta = 45^\circ$ and $f = 1$ THz, $\frac{1}{\kappa} = 0.0135$ cm. Namely, the transmitted field very quickly decays, and therefore, due to the imaginary value of $\cos\phi$, the average of the transmitted Poynting vector is zero. Thus, we can safely say that the transmission probability to vacuum $T = 0$ and the absorptance (A) can be directly obtained from the reflectance (R), i.e., $A = 1 - R$. At $\theta = \theta_c$, $\cos\phi = 0$, and from Eqs. (3)

and (4) we get $R_p = 1$ for any value of Z_1, while R_s depends on σ, Z_1, and Z_2.

R_p and R_s are plotted as a function of frequency in Figure 3(d) and as a function of angle θ in Figure 4(b). Here we used $n_1 = 1.523$, $n_2 = 1$, $E_{\mathrm{F}} = 0.308$ eV, and $\mu = 1.07 \times 10^3\,\mathrm{cm^2V^{-1}s^{-1}}$. From Figure 2(a), we know that the conductivity is constant between 0.4 and 1.5 THz, which is the frequency range of interest for our THz absorption enhancement measurements, and therefore, in the calculations we simply used $f = 1\,\mathrm{THz}$. The reason why we measured the conductivity for such a broad frequency range was for obtaining the Fermi energy and relaxation time parameters through Drude-model fitting. The calculated spectra reproduce the experiment results well, as shown Figure 4(b). At relatively large θ ($64^\circ - 68^\circ$), however, the experimental values are systematically higher than the calculated values; we presently do not have an explanation for this slight discrepancy. From the calculation, we know that the absorption of light by graphene is significantly enhanced within the THz range. The calculated results shows that the R_p has a minimum of around 61% at $\theta = 55^\circ$, while R_s increases from 25% at right above $\theta = \theta_c$ monotonically with increasing θ, which agrees with the experiment. The maximum absorptance of $p(s)$-polarized wave can be around 39%(75%) within the THz range, in contrast to the well-known 2.3% absorptance for visible light.

The calculated results also show that in general R_s is lower than R_p, which implies that an s-polarized THz wave is more strongly absorbed by monolayer graphene than a p-polarized THz wave. The absorption of a THz wave can be understood as a dissipative (or Ohmic) loss through Joule heating that occurs in graphene. For our geometry, we expect stronger Joule heating induced by an s-polarized wave than by a p-polarized wave. We will now show that the absorptance is proportional to the amount of Joule heating. The Joule heat, q_k, in units of $\mathrm{W\,m^{-2}}$ can be expressed as

$$q_k = \frac{1}{2}\,\mathrm{Re}\left[\sigma^* \left|E_{gk}\right|^2\right], \tag{8}$$

where E_{gk} is the electric field on the graphene surface for a k-polarized wave ($k = p, s$),

which can be written as

$$E_{gp} = (E_i + E_r)\cos\theta = (1 + r_p)\cos\theta E_i \tag{9}$$

$$E_{gs} = (E_i + E_r) = (1 + r_s)\, E_i, \tag{10}$$

where r_k $(k = p, s)$ can be obtained from Eqs. (3) and (4). The Joule heat, q_k, can be calculated by substituting Eqs. (9) and (10) into Eq. (8). We define a dimensionless quantity, $Q_k \equiv q_k/I_i$, which is the ratio of the Joule heat to the incident intensity $\left(I_i = \frac{|E_i|^2}{2Z_1}\cos\theta \ \ [\mathrm{Wm}^{-2}]\right)$. We can express the Q_k as

$$Q_p = \frac{4Z_1 Z_2^2 \cos\theta \left|\cos\phi\right|^2 \Re\left[\sigma^*\right]}{\left|Z_2\cos\phi + Z_1\cos\theta + \sigma Z_1 Z_2 \cos\theta\cos\phi\right|^2}, \tag{11}$$

$$Q_s = \frac{4Z_1 Z_2^2 \cos\theta \Re\left[\sigma^*\right]}{\left|Z_2\cos\theta + Z_1\cos\phi + \sigma Z_1 Z_2\right|^2}. \tag{12}$$

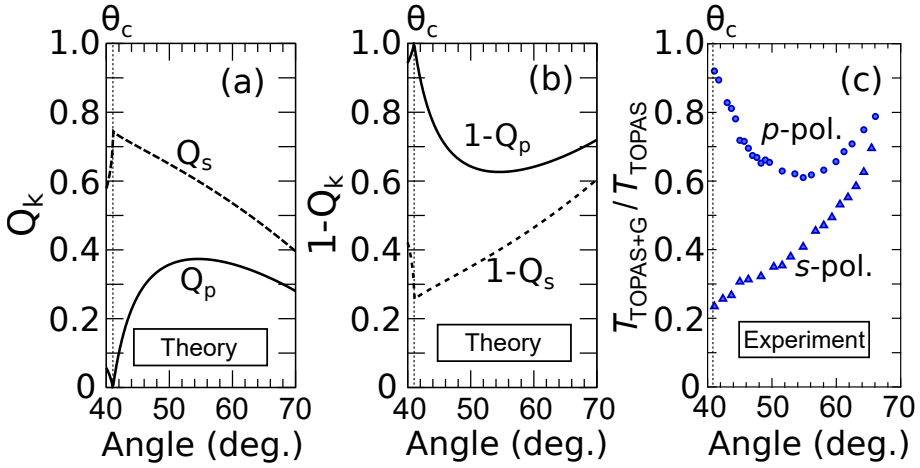

Figure 6: (a) The calculated plot of $Q_k \equiv q_k/I_i$ $(k = p, s)$, which is the ratio of Joule's heat to the incident intensity, (b) and of $1 - Q_k$ for both polarizations. (c) Experimentally observed $T_{\mathrm{TOPAS+G}}/T_{\mathrm{TOPAS}}$.

The calculated Q_p and Q_s are plotted as a function of θ in Figure 6(a) as solid and dashed line, respectively. We can see that Q_s is larger than Q_p at all angles, which means that Joule heating in graphene by an s-polarized wave is higher than that by a p-polarized

wave. We also plot $1 - Q_k$ $(k = p, s)$ in Figure 6(b). The calculated $1 - Q_k$ spectra for $\theta > \theta_c$ reproduce quite well the observed and calculated $T_{\mathrm{TOPAS+G}}/T_{\mathrm{TOPAS}}$ spectra for both polarizations, which is shown in Figures 4 and 6(c). This means that Q_k $(k = p, s)$ is nothing but the absorptance itself and that the absorption can be quantified by the Joule heat. Therefore, Eqs. (11) and (12) are the analytical expressions of the absorptance for both polarizations; hence, from now on, we refer to Q_k as absorptance.

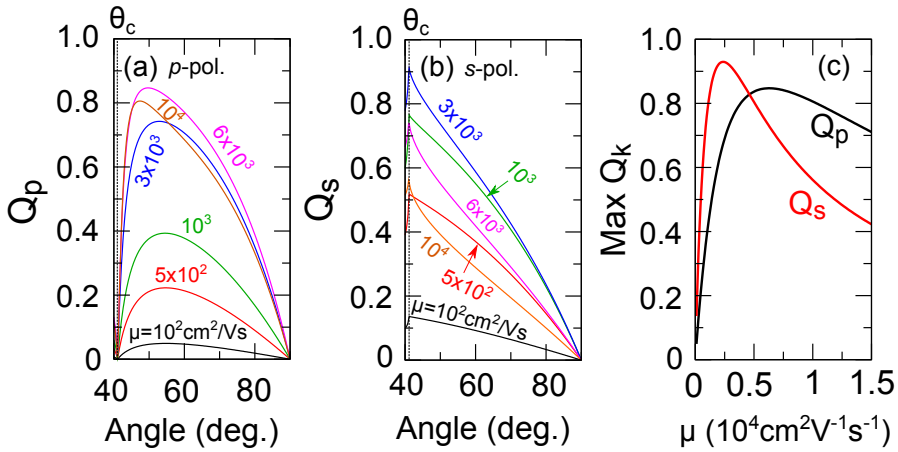

Figure 7: The calculated absorptance Q_k $(k = p, s)$ with several graphene mobilities μ and fixed $E_{\mathrm{F}} = 0.308$ eV for (a) p-polarization, (b) s-polarization. (c) Maximum value of Q_k as a function of μ.

In our experiments, we used a graphene sample with $\mu = 1.07 \times 10^3\,\mathrm{cm^2V^{-1}s^{-1}}$ and $E_{\mathrm{F}} = 0.308\,\mathrm{eV}$. Below, we theoretically show how Q_k should depend on μ and E_{F}. In Figure 7, we show the calculated Q_k for both polarizations with several assumed values of μ and a fixed E_{F} of $0.308\,\mathrm{eV}$. From Figure 7(a), we can see that Q_p increases as μ increases; for example, Q_p can reach a maximum of $\sim 85\%$ if $\mu = 6 \times 10^3\,\mathrm{cm^2V^{-1}s^{-1}}$, in contrast to $\sim 39\%$ in our graphene sample. However, increasing μ does not always increase Q_p, as we see in the case of $\mu = 10^4\,\mathrm{cm^2V^{-1}s^{-1}}$, where $Q_p(\mu = 10^4\,\mathrm{cm^2V^{-1}s^{-1}})$ is smaller than $Q_p(\mu = 6 \times 10^3\,\mathrm{cm^2V^{-1}s^{-1}})$. The same trend also occurs in the case of s-polarization, which is shown in Figure 7(b). This can be understood from Eqs. (11) and (12) by taking $\frac{\partial Q_k}{\partial \theta} = 0$ to find the maximum value of Q_k. In Figure 7(c), we show the numerical results of maximum value of Q_k as a function of μ for both polarizations. We see that $Q_p(Q_s)$ saturates at

$\mu \sim 6 \times 10^3\,(2.5 \times 10^3)\,\mathrm{cm^2V^{-1}s^{-1}}$, where $Q_p(Q_s)$ starts to decrease if μ is increased. From Figure 7, we can also see that the absorptance of an s-polarized wave can be lower than that of a p-polarized wave if μ is relatively high. This is shown in Figures 7(a) and (b) for the case of $\mu = 6 \times 10^3$ and $10^4\,\mathrm{cm^2V^{-1}s^{-1}}$, where Q_s is smaller than Q_p for all θ, and more generally in Figure 7(c) for $\mu > 5 \times 10^3\,\mathrm{cm^2V^{-1}s^{-1}}$, where the maximum value of Q_s is smaller than that of Q_p.

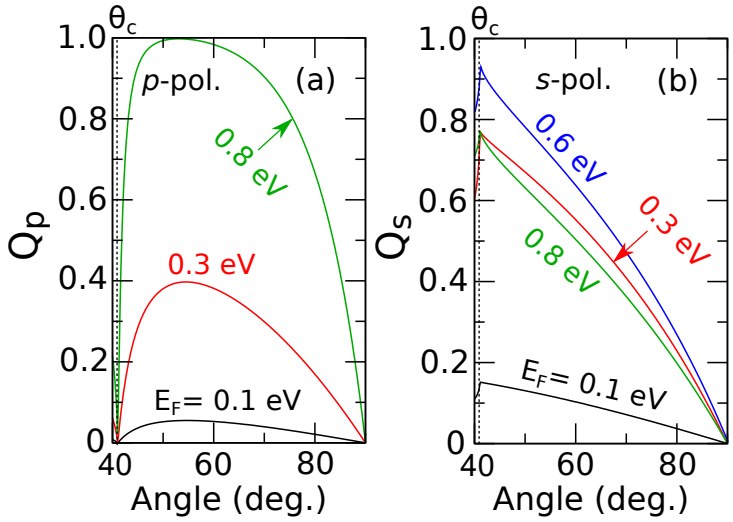

Figure 8: The calculated absorptance Q_k $(k = p, s)$ with several E_F and fixed $\mu = 1.07 \times 10^3\mathrm{cm^2V^{-1}s^{-1}}$ for (a) p-polarization, (b) s-polarization.

In Figure 8, we show the calculated Q_k $(k = p, s)$ with several E_F and fixed $\mu = 1.07 \times 10^3\,\mathrm{cm^2V^{-1}s^{-1}}$ for both polarizations. From Figure 8(a), Q_p for all θ increases as we increase E_F. Q_p even reaches 100% at $E_\mathrm{F} = 0.8$ eV, in contrast to $\sim$ 39% maximum Q_p of our graphene sample, which has $E_\mathrm{F} \approx 0.3$ eV. Therefore, to obtain total absorption of a p-polarized wave by monolayer graphene with $\mu = 1.07 \times 10^3\,\mathrm{cm^2V^{-1}s^{-1}}$, a relatively high E_F is needed. Increasing E_F also increases Q_s for all θ, which is shown in Figure 8(b). However, increasing E_F more than 0.6 eV will decrease Q_s, as we see in the case of $E_\mathrm{F} = 0.8$ eV, $Q_s(E_\mathrm{F} = 0.8\text{ eV}) < Q_s(E_\mathrm{F} = 0.6\text{ eV})$.

Methods

THz time-domain spectroscopy

For generating and detecting THz waves in performing THz time-domain spectroscopy measurements, we used a commercial instrument (Advantest/TAS7400TS, Advantest Corporation) equipped with compact fiber-coupled photoconductive switch emitter and detector, which allowed us to couple the THz beam into the graphene-on-TOPAS structure with minimum effort. The THz wave coming out of the emitter fiber was collimated and focused onto the graphene-on-TOPAS structure by a pair of off-axis parabolic mirrors; the beam after the structure was then recollimated and focused onto the detector fiber by using another pair of off-axis parabolic mirrors. In order to adjust the beam diameter, we put an iris in front of the structure. In addition, the setup was covered by a dry-air purge box for minimizing atmospheric absorption. Figure 9 shows a schematic diagram of the experimental setup, together with typical frequency-domain and time-domain data.

Additionally, we constructed a setup to evaluate the amount of any THz radiation leaking out of the waveguide structure by inserting metal plates in certain locations to prevent any leaked THz radiation from hitting the detector. Then, we compared data with and without the metal blocks and concluded that there was no difference between the two within the experimental uncertainties as long as the incidence angle was above the critical angle. These additional measurements ensured that we analyzed only the THz beam that experienced the desired, perfect total internal reflections.

Chemical vapor deposition

We used conventional chemical vapor deposition (CVD) methods for growing monolayer graphene on a 25-μm-thick Cu foil (99.8%, Alfa-Aesar). Before the growth process, the Cu foil was first thoroughly cleaned by sonication in 100-mL acetone for 30 minutes, washed by 200-mL isopropyl alcohol (IPA) 3 times and 200-mL deionized (DI) water 3 times, and

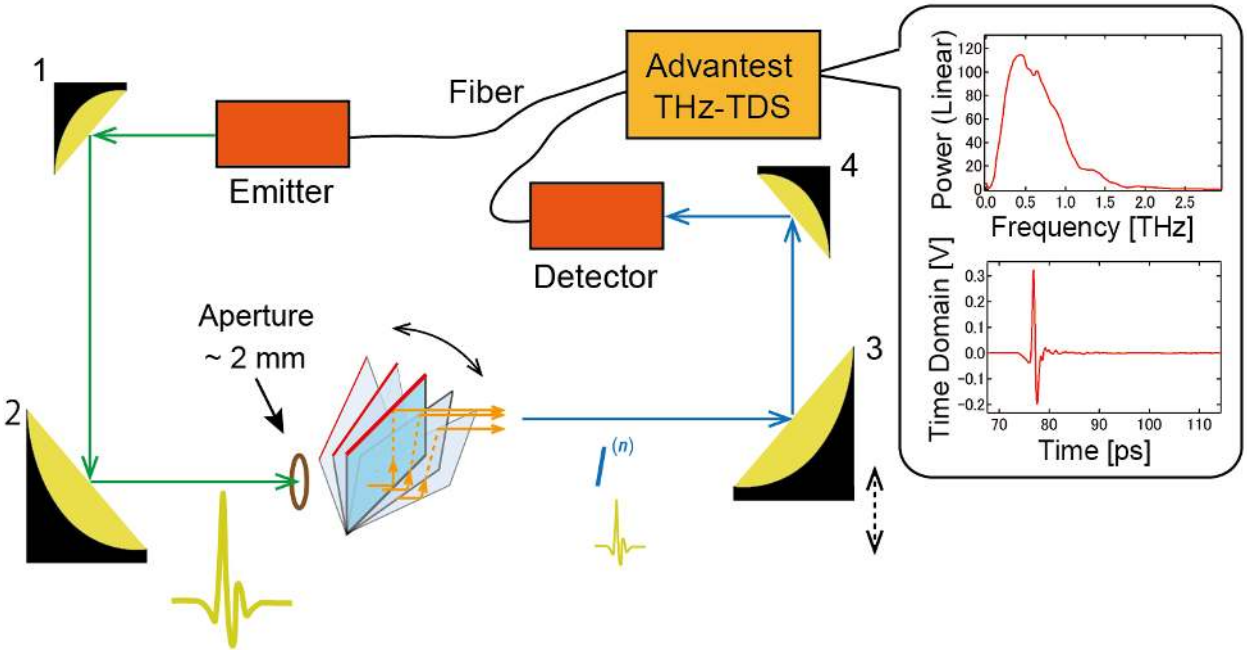

Figure 9: Experimental setup used for THz time-domain spectroscopy of the graphene-on-TOPAS samples. The figures on the right show typical frequency-domain (top) and time-domain (bottom) traces.

then dried in a dry-air flow for 3 minutes. The cleaned Cu foil was further polished using an electrochemical method. After that, the Cu foil was moved into a hot region of the furnace at a temperature of 950–1050 °C for 20 minutes to 4 hours to anneal the Cu substrate.

Transfer

A wet-etch method was used for transferring graphene from the Cu foil to the TOPAS waveguide structure. First, 300 μL PMMA (4% in anisole) solution was put on the top of the Cu foil. The PMMA/graphene/foil was cut into 5.5×5.5-mm^2-sized pieces and then spin-coated at 3000 rpm for 60 seconds. After the Cu foil was dissolved by using an etchant (667528 ALDRICH Copper etchant), we used the TOPAS waveguide for picking up the floating PMMA/graphene film. The PMMA/graphene/TOPAS structure was then left in air for 10 hours and then vacuum dried at 70 °C for 2 hours. Finally, the sample was rinsed with acetone for 60 seconds for 3 times and further rinsed with IPA for 3 times to dissolve

the PMMA layer.

Acknowledgement

Work performed at Rice University was supported by the Robert A. Welch Foundation through grant no. C-1509. M.S.U. and E.H.H. acknowledge the MEXT scholarship. A.R.T.N. was supported by the Leading Graduate School Program at Tohoku University. R.S. acknowledges MEXT (Japan) Grants No. 25107005 and No. 25286005.

References

(1) Otsuji, T.; Boubanga-Tombet, S. A.; Satou, A.; Fukidome, H.; Suemitsu, M.; Sano, E.; Popov, V.; Ryzhii, M.; Ryzhii, V. Graphene-Based Devices in Terahertz Science and Technology. *J. Phys. D: Appl. Phys.* **2012**, *45*, 303001.

(2) Tassin, P.; Koschny, T.; Soukoulis, C. M. Graphene for Terahertz Applications. *Science* **2013**, *341*, 620–621.

(3) Hartmann, R. R.; Kono, J.; Portnoi, M. E. Terahertz Science and Technology of Carbon Nanomaterials. *Nanotechnology* **2014**, *25*, 322001.

(4) Horng, J.; Chen, C.-F.; Geng, B.; Girit, C.; Zhang, Y.; Hao, Z.; Bechtel, H. A.; Martin, M.; Zettl, A.; Crommie, M. F.; Shen, Y. R.; Wang, F. Drude Conductivity of Dirac Fermions in Graphene. *Phys. Rev. B* **2011**, *83*, 165113.

(5) Yan, H.; Xia, F.; Zhu, W.; Freitag, M.; Dimitrakopoulos, C.; Bol, A. A.; Tulevski, G.; Avouris, P. Infrared Spectroscopy of Wafer-Scale Graphene. *ACS Nano* **2011**, *5*, 9854–9860.

(6) Ren, L.; Zhang, Q.; Yao, J.; Sun, Z.; Kaneko, R.; Yan, Z.; Nanot, S.; Jin, Z.; Kawayama, I.; Tonouchi, M.; Tour, J. M.; Kono, J. Terahertz and Infrared Spectroscopy of Gated Large-Area Graphene. *Nano Lett.* **2012**, *12*, 3711–3715.

(7) Maeng, I.; Lim, S.; Chae, S. J.; Lee, Y. H.; Choi, H.; Son, J.-H. Gate-Controlled Nonlinear Conductivity of Dirac Fermion in Graphene Field-Effect Transistors Measured by Terahertz Time-Domain Spectroscopy. *Nano Lett.* **2012**, *12*, 551–555.

(8) Sensale-Rodriguez, B.; Yan, R.; Kelly, M. M.; Fang, T.; Tahy, K.; Hwang, W. S.; Jena, D.; Liu, L.; Xing, H. G. Broadband Graphene Terahertz Modulators Enabled by Intraband Transitions. *Nat. Commun.* **2012**, *3*, 780.

(9) Mics, Z.; Tielrooij, K.-J.; Parvez, K.; Jensen, S. A.; Ivanov, I.; Feng, X.; Müllen, K.; Bonn, M.; Turchinovich, D. Thermodynamic Picture of Ultrafast Charge Transport in Graphene. *Nat. Commun.* **2015**, *6*, 7655.

(10) Nikitin, A. Y.; Guinea, F.; Garcia-Vidal, F. J.; Martin-Moreno, L. Surface Plasmon Enhanced Absorption and Suppressed Transmission in Periodic Arrays of Graphene Ribbons. *Phys. Rev. B* **2012**, *85*, 081405.

(11) Thongrattanasiri, S.; Koppens, F. H. L.; García de Abajo, F. J. Complete Optical Absorption in Periodically Patterned Graphene. *Phys. Rev. Lett.* **2012**, *108*, 047401.

(12) Piper, J. R.; Fan, S. Total Absorption in a Graphene Monolayer in the Optical Regime by Critical Coupling with a Photonic Crystal Guided Resonance. *ACS Photon.* **2014**, *1*, 347–353.

(13) Shoufie Ukhtary, M.; Hasdeo, E. H.; Nugraha, A. R. T.; Saito, R. Fermi Energy-Dependence of Electromagnetic Wave Absorption in Graphene. *Appl. Phys. Exp.* **2015**, *8*, 055102.

(14) D'Angelo, F.; Mics, Z.; Bonn, M.; Turchinovich, D. Ultra-broadband THz Time-Domain Spectroscopy of Common Polymers Using THz Air Photonics. *Opt. Exp.* **2014**, *22*, 12475–12485.

(15) Luican, A.; Li, G.; Andrei, E. Y. Quantized Landau Level Spectrum and its Density Dependence in Graphene. *Phys. Rev. B* **2011**, *83*, 041405.

Graphical TOC Entry